Electronic Supplementary Material (ESI) for Journal of Materials Chemistry A.

Defect-engineered vanadium trioxide nanofiber bundle@graphene hybrids for high-performance all-vanadate Na-ion and K-ion full batteries

Zhongqiu Tong,[ab] Rui Yang,[ab] Shilin Wu,[bc] Dong Shen,[ab] Tianpeng Jiao,[bc] Kaili Zhang,[d] Wenjun Zhang,[bc] Chun-Sing Lee[*] [ab]

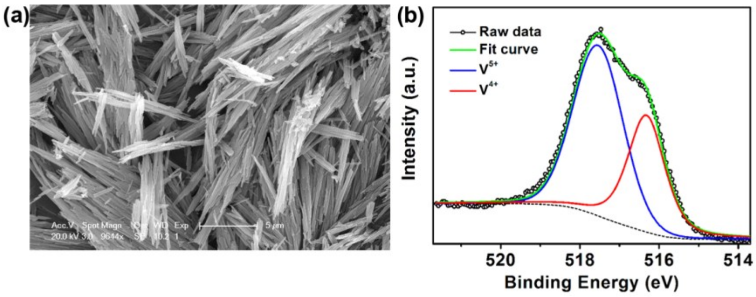

Fig. S1 SEM image (a) and V $2p_{3/2}$ XPS data (b) of VO_x sample.

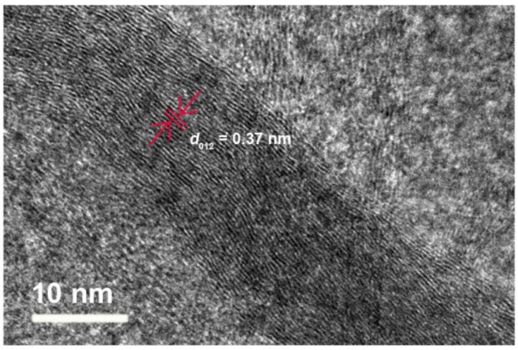

Fig. S2 HRTEM image of V_2O_{3-x} sample.

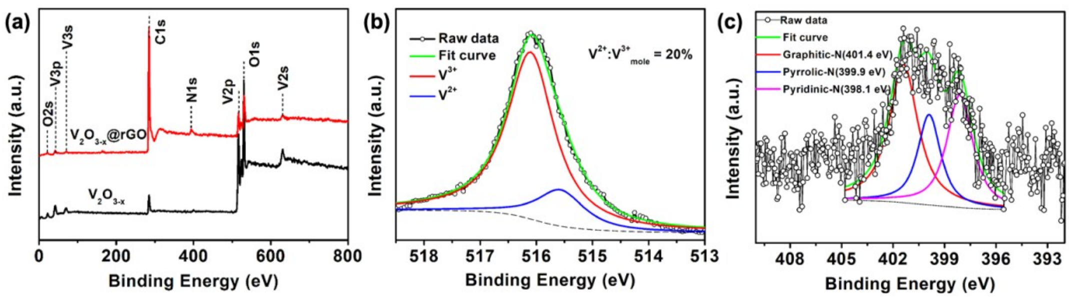

Fig. S3 (a) XPS data of V_2O_{3-x}@rGO and V_2O_{3-x} samples. (b) V $2p_{3/2}$ XPS data of V_2O_{3-x}. (c) N 1s XPS spectra of V_2O_{3-x}@rGO sample.

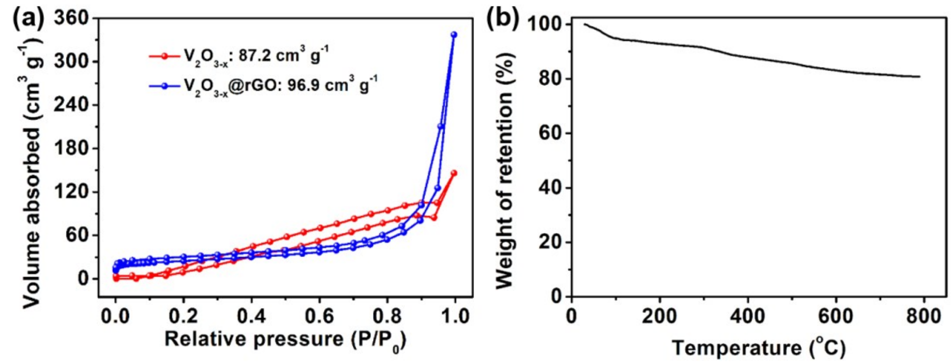

Fig. S4 (a) Nitrogen adsorption/desorption isotherms of V_2O_{3-x} and V_2O_{3-x}@rGO. (b) TGA data of the V_2O_{3-x}@rGO in air.

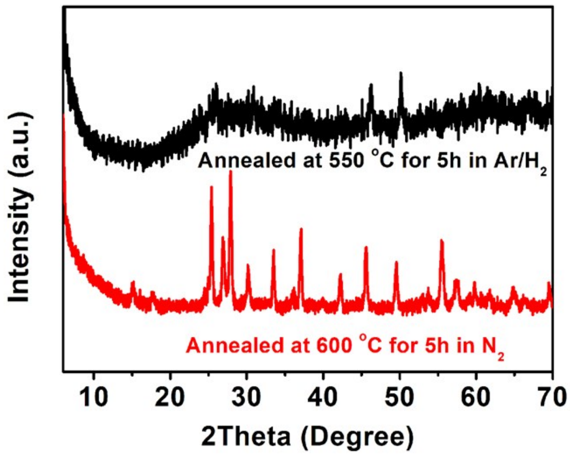

Fig. S5 XRD patterns of vanadium oxide samples annealed at 550 ^oC for 5 h in Ar/H_2 and at 600 ^oC for 5 h in N_2.

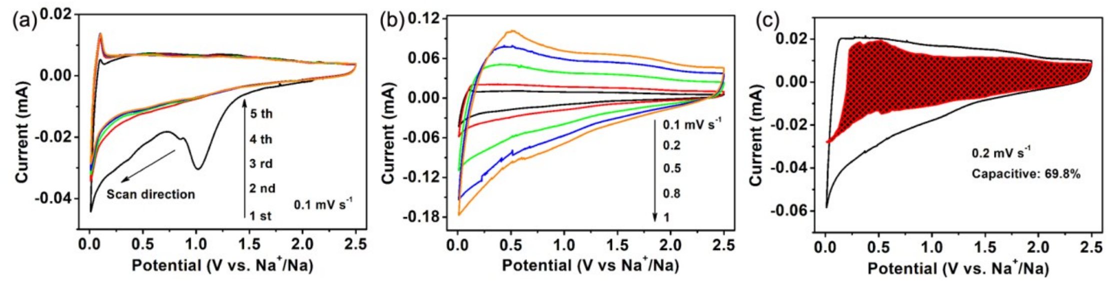

Fig. S6 Na-ion insertion/release redox performance of the V_2O_{3-x}@rGO. CVs of the V_2O_{3-x}@rGO electrode at the scan rates of 0.1 mV s^{-1} (a) and various scan rates (b). (c) CV curve of the V_2O_{3-x}@rGO electrode with separation between total current and surface capacitive current (shaded regions) at 0.2 mV s^{-1}. The current is quantitatively deconvoluted based on equation: $i(V) = k_1 v + k_2 v^{1/2}$, where $i(V)$ is the measured current at a fixed potential (V) under a certain sweep rate, k_1 and k_2 are adjustable values.

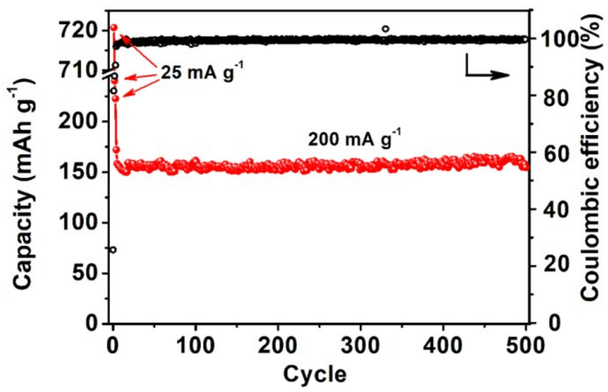

Fig. S7 Cycling performance at 200 mA g^{-1} of V_2O_{3-x}@rGO Na-ion half cell.

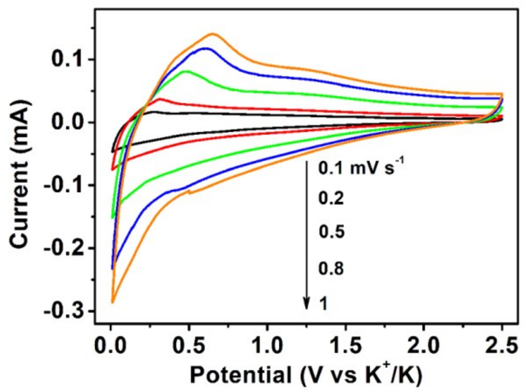

Fig. S8 CVs of the V_2O_{3-x}@rGO K storage anode at various scan rates.

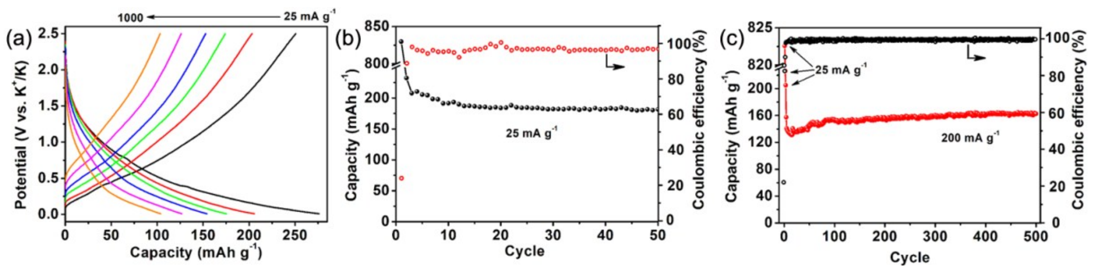

Fig. S9 K-ion insertion/extraction performance of V_2O_{3-x}@rGO K-ion half cells. (a) Rate curves of the V_2O_{3-x}@rGO electrode at various current densities. (b,c) Cycling performance at 25 and 200 mA g^{-1}, respectively.

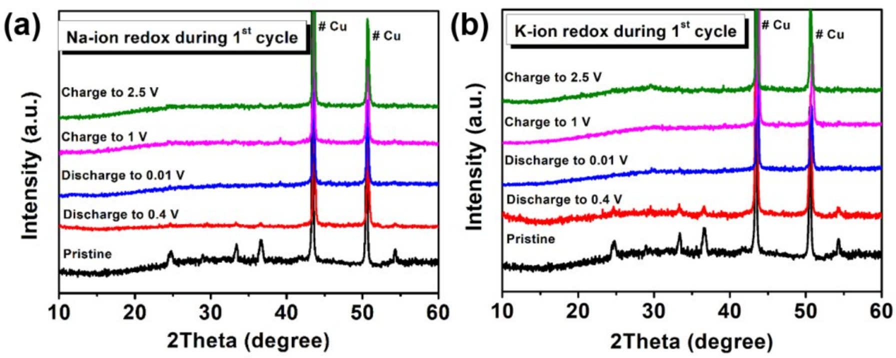

Fig. S10 *Ex situ* XRD patterns obtained at various states during the first discharge/charge cycle of V_2O_{3-x} electrodes for Na-ion (a) and K-ion (b) storage. Given the strength of XRD peaks of V_2O_{3-x} sample was weak, electrodes for *Ex situ* XRD were prepared by mixing the V_2O_{3-x} and PVDF without super P.

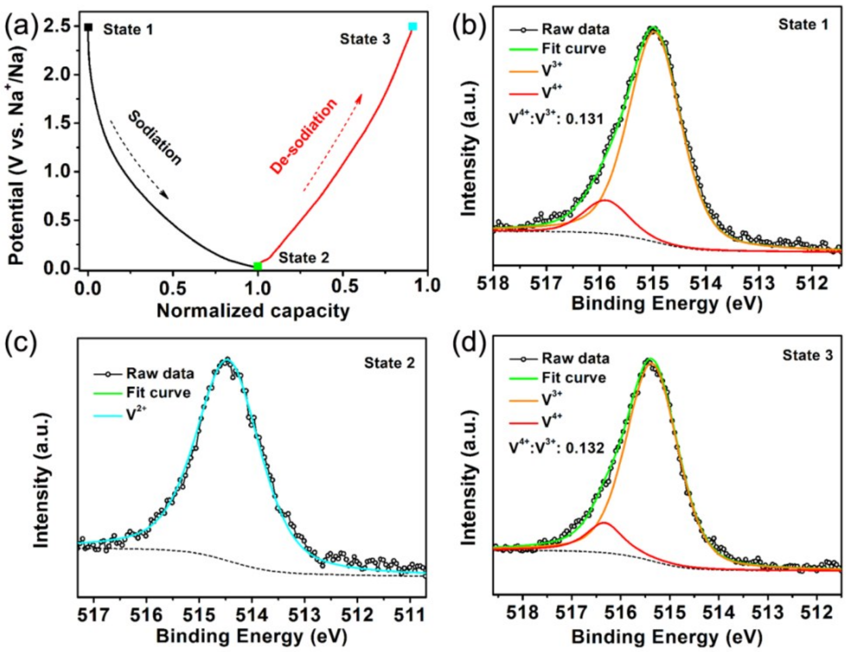

Fig. S11 XPS studies of the V_2O_{3-x}@rGO Na-ion anodes. (a) Voltage profiles of the black Nb_2O_{5-x}@rGO nanosheets in different stages of discharge/charge at which the samples were taken for ex situ XPS test. (b,c,d) V $2p_{3/2}$ peaks at the initial 2.5 V, fully discharged 0.01 V, and fully charged 2.5 V states, respectively.

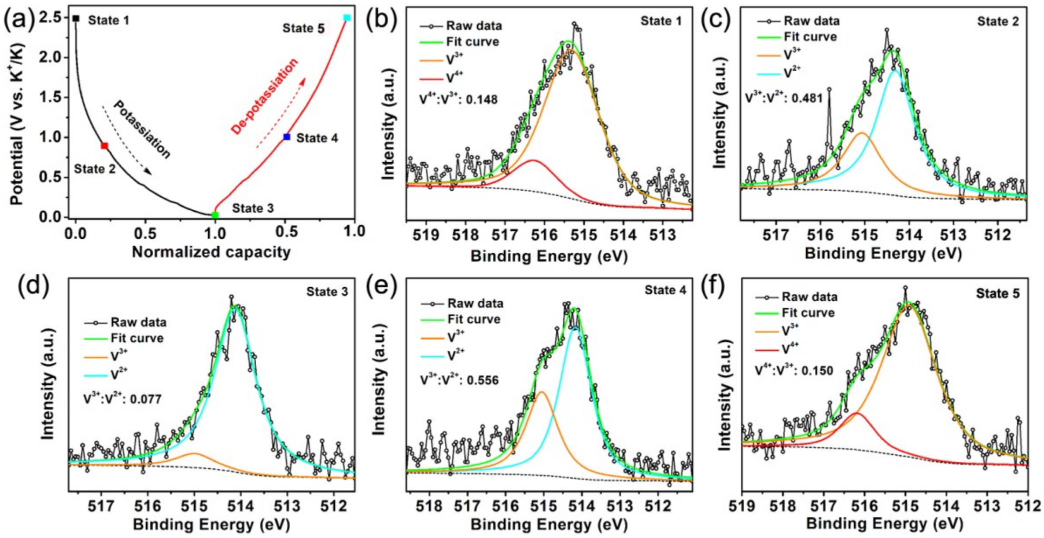

Fig. S12 XPS studies of the V_2O_{3-x}@rGO K-ion anodes. (a) Voltage profiles of the black Nb_2O_{5-x}@rGO nanosheets in different stages of discharge/charge at which the samples were taken for ex situ XPS test. (b,c,d,e,f) V $2p_{3/2}$ peaks at the initial 2.5 V, discharged 0.9 V, fully discharged 0.01 V, charged 1 V, and fully charged 2.5 V states, respectively.

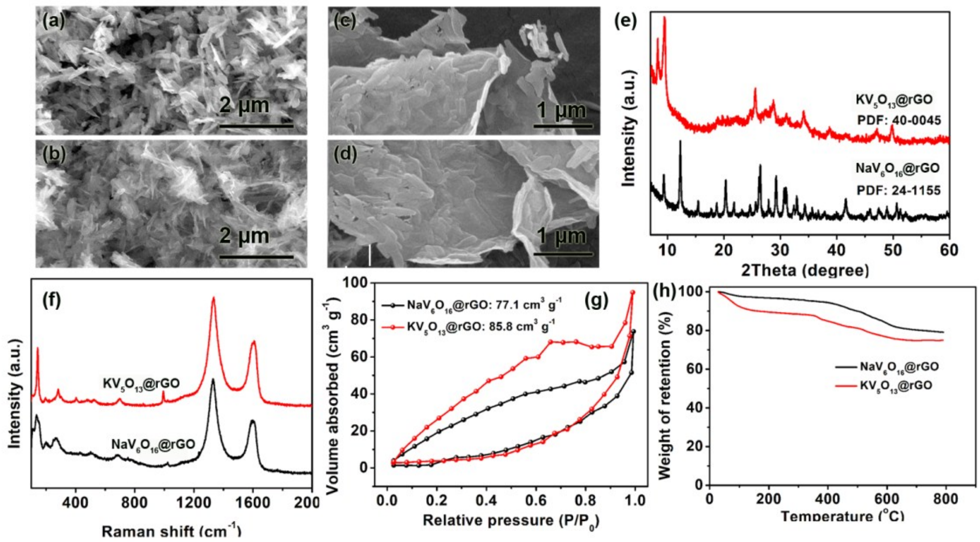

Fig. S13 Physical characterization about the NaVO@rGO and KVO@rGO cathodes. (a,b,c,d) SEM images of KVO, NaVO, KVO@rGO, and NaVO@rGO samples, respectively. (e,f,g,h) XRD patterns, Raman spectra, nitrogen adsorption/desorption isotherms, and TGA curves of KVO@rGO, and NaVO@rGO samples, respectively.

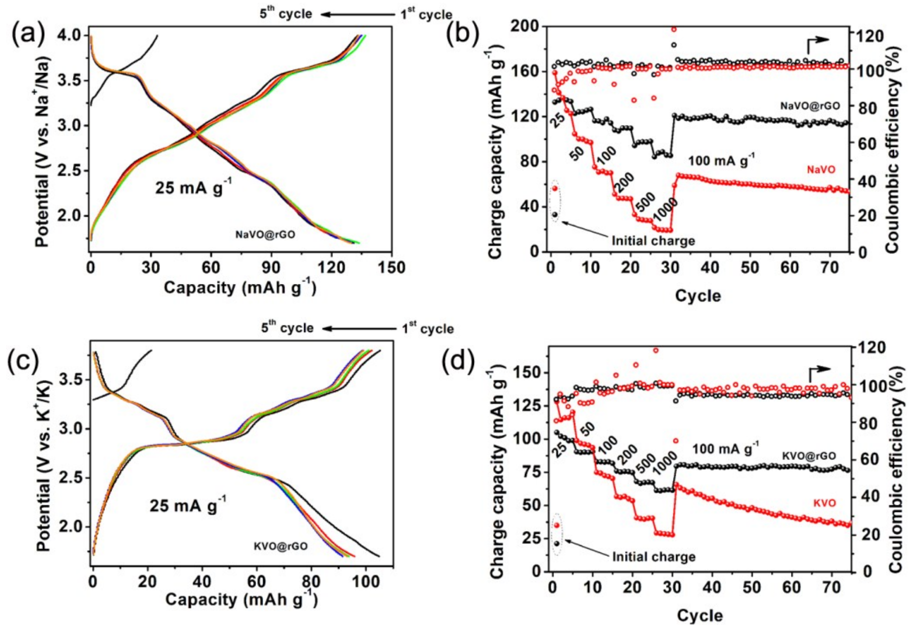

Fig. S14 (a,b) First five discharge/charge curves at 25 mA g^{-1} and rate performance of NaVO@rGO electrodes, respectively. (c,d) First five discharge/charge curves at 25 mA g^{-1} and rate performance of KVO@rGO electrodes, respectively.

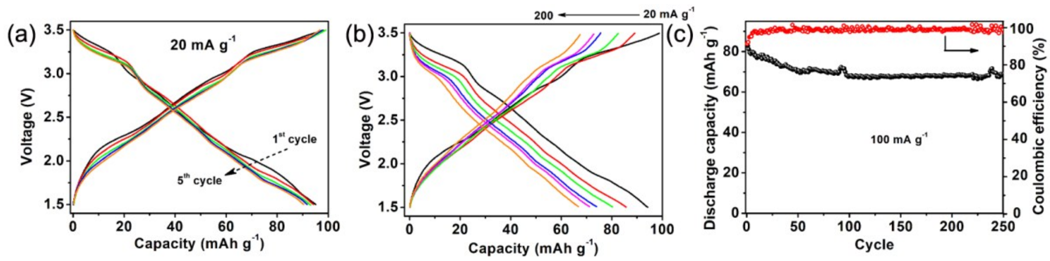

Fig. S15 (a,b,c) First five discharge/charge curves at 20 mA g^{-1}, rate curves (20, 40, 60, 80, 100, and 200 mA g^{-1}), and cycling stability of V_2O_{3-x}@rGO//KVO@rGO SIBs, respectively.

Table S1. Comparison of the electrochemical performances of V_2O_{3-x}@rGO anodes with recently reported V_2O_3 and typical metal oxide anodes.

Active materials	Stored alkali metal ion	Current density (mA g^{-1})	Discharge capacity (mAh g^{-1})	Reference
V_2O_{3-x}@rGO	Na	200 1000	151 101	This work
V_2O_{3-x}@rGO	K	200 1000	162 104	This work
V_2O_3/C core/shell nanofiber	Li	1000	145	[1]
Polycrystalline V_2O_3 nanorod	Li	1200	100	[2]
$Na_6[V_{10}O_{28}]$ polyoxometalate	Na	200	~100	[3]
V_2O_3 nanoparticle	Na	1000	50	[4]
V_2O_3@carbon nanocomposites	Na	1000	120	[4]
V_2O_3@graphene nanobelts	Na	1000	115	[5]
Quantum V_2O_3@carbon	Na	1000	140	[6]
$K_{0.23}V_2O_5$ nanoplates	K	400	92	[7]
V_2O_3@PNCNFs	K	50 1000	240 114	[8]
$K_2Ti_8O_{17}$ nanorod clusters	K	200	~90	[9]
$KTi_2(PO_4)_3$ nanocubes	K	64	~75.6	[10]
$K_{0.6}Mn_1F_{2.7}$ hollow nanocubes	K	200 1000	118 78	[11]
Porous carbon Fe_3O_4	K	200	127	[12]

Reference for Table S1:

1. X. Li, J. Fu, Z. Pan, J. Su, J. Xu, B. Gao, X. Peng, L. Wang, X. Zhang, P. K. Chu, J. Power Sources, 2016, 331, 58-66.
2. D. McNulty, D. N. Buckley, C. O’Dwyer, ChemElectroChem, 2017, 4, 2037-2044.
3. S. Hartung, N. Bucher, H. Chen, R. Al-Oweini, S. Sreejith, P. Borah, Z. Yanli, U. Kortz, U. Stimming, H. E. Hoster, M. Srinivasan, J. Power Sources, 2015, 288,270-277.
4. X. An, H. Yang, Y. Wang, Y. Tang, S. Liang, A. Pan, G. Cao, Sci. China Mater., 2017, 60, 717-727.
5. J. Zhang, Q. Li, Z. Liao, L. Wang, J. Xu, X. Ren, B. Gao, P. K. Chu, K. Huo, ChemElectroChem, 2018, 5, 1387-1393.
6. Y. Cai, G. Fang, J. Zhou, S. Liu, Z. Luo, A. Pan, G. Cao, S. Liang, Nano Res., 2018, 11, 449-463.
7. C. Liu, S. Luo, H. Huang, Z. Wang, Q. Wang, Y. Zhang, Y. Liu, Y. Zhai, Z. Wang, J. Power Sources, 2018, 389, 77-83.
8. T. Jin, H. Li, Y. Li, L. Jiao, J. Chen, Nano Energy, Nano Energy, 2018, 50, 462-467.
9. J. Han, M. Xu, Y. Niu, G. Li, M. Wang, Y. Zhang, M. Jia, C. Li, Chem. Commun., 2016,52, 11274-11276.
10. J. Han, Y. Niu, S. Bao, Y. Yu, S. Lu, M. Xu, Chem. Commun., 2016, 52, 11661-11664.

11. Z. W. Liu, P. Li, G. Q. Suo, S. Gong, W. (Alex) Wang, C. Y. Lao, Y. J. Xie, H. Guo, Q. Y. Yu, W. Zhao, K. Han, Q. Wang, M. L. Qin, K. Xi, X. H. Qu, Energy Environ. Sci., 2018, 11, 3033 -3042.
12. J. Ming, H. Ming, W. Yang, W. Kwak, J. Park, J. Zheng, Y. Sun, RSC Adv., 2015, 5, 8793-8800.

Table S2. Comparison of the electrochemical performances of reported full PIBs.

Active materials (anode//cathode)	Potential window	Cycling current density (mA g^{-1})	Cycling number	Initial discharge capacity/cycling retention (mAh g^{-1})	Reference
V_2O_{3-x}@rGO//KV_5O_{13}	1.5-3.1 V	100	250	51.4/75.1%	This work
$K_{0.7}Fe_{0.5}Mn_{0.5}O_2$//soft carbon	0.5-3.5 V	100	250	48/76%	[2]
$K_{0.6}CoO_2$// hard carbon	0.5-3.8 V	30	100	72/79%	[3]
$K_{0.51}V_2O_5$//graphite	1.8-3.9 V	300	100	80/84%	[4]
$K_{0.3}MnO_2$//hard carbon-carbon black	0.5-3.4 V	32	100	82/51%	[10]
$K_{1.92}Fe[Fe(CN)_6]_{0.94}\cdot 0.5H_2O$//Dipotassium terephthalate	1.5-3.8 V	60	65	110/90%	[14]
$K_{0.6}CoO_2$// soft carbon	0.5-3.5 V	20	50	84/84%	[1]
$K_{0.22}Fe[Fe(CN)_6]_{0.805}\cdot 4.01H_2O$//Super P	1-3.8 V	100	50	73/89%	[8]
$K_3V_2(PO_4)_2F_3$//graphite	1.5-4.6 V	10	50	84/70%	[12]
K2C6O6//K2C6O6	0.5-2 V	25	10	70/61%	[11]
$K_{1.98}Mn[Fe(CN)_6]_{0.92}$//$WS_2$	2-4 V	10	10	40/80%	[9]
$K_{0.6}CoO_2$//graphite	0.5-3.8 V	3	5	53/47%	[13]

Reference for Table S2:

1. X. Wang, K. Han, D. Qin, Q. Li, C. Wang, C. Niu, L. Mai, Nanoscale, 2017, 9, 18216-18222.
2. X. Wang, X. Xu, C. Niu, J. Meng, M. Huang, X. Liu, Z. Liu, L. Mai, Nano Lett., 2017, 17, 544–550.
3. T. Deng, X. Fan, C. Luo, J. Chen, L. Chen, S. Hou, N. Eidson, X. Zhou and C. Wang, Nano Lett., 2018, 18, 1522–1529.
4. Y. Zhu, Q. Zhang, X. Yang, E. Zhao, T. Sun, X. Zhang, S. Wang, X. Yu, J. Yan, Q. Jiang, Chem, 2019, 5, 1-12.
5. Y. Fang, L. Xiao, J. Qian, Y. Cao, X. Ai, Y. Huang, H. Yang, Adv. Energy Mater., 2016, 6, 1502197.
6. X. Wang, S. Kajiyama, H. Linuma, E. Hosono, S. Oro, I. Moriguchi, M. Okubo, A. Yamada, Nat. Commun., 2015, 6, 6544.
7. Z. Zhu, F. Cheng, Z. Hu, Z. Niu, J. Chen, J. Power Sources, 2015, 293, 626-634.
8. C. Zhang, Y. Xu, M. Zhou, Y. Liang, H. Dong, M. Wu, Y. Yang, Y. Lei, Adv. Funct. Mater., 2017, 27, 1604307.
9. R. Zhang, J. Bao, Y. Pan, C. Sun, Chem. Sci., 2019, DOI: 10.1039/c8sc04350g.
10. C. Vaalma, G. Giffin, D. Buchholz, S. Passerinia, J. Electrochem. Soc., 2016, 163,

A1295-A1299.
11. Q. Zhao, J. Wang, Y. Lu, Y. Li, G. Liang, J. Chen, Angew. Chem. Int. Ed., 2016, 55, 12528-12532.
12. X. Lin, J. Huang, H. Tan, J. Huang, B. Zhang, Energy Storage Mater., 2019, 16, 97-101.
13. H. Kim, J. Kim, S. Bo, T. Shi, D. Kwon, G. Cede, Adv. Energy Mater. 2017, 7, 1700098
14. J. Liao, Q. Hu, Y. Yu, H. Wang, Z. Tang, Z. Wen, C. Chen, J. Mater. Chem. A, 2017, 5, 19017.